Caving 2010 — Y. Potvin (ed)

doi:10.36487/ACG_rep/1002_36_Bsainsbury

Sensitivities in the numerical assessment of cave propagation

B.L. Sainsbury *Itasca Australia Pty Ltd; and The University of New South Wales, Australia*

Abstract

The accurate assessment of cave initiation and propagation is of critical importance to the planning of any new caving operation. For this reason, the use of numerical models for simulation of the undercutting, draw, propagation and surface subsidence processes are becoming more commonplace. This paper describes the application of a numerical caving algorithm that has been developed within the industry funded Mass Mining Technology (MMT) project. The caving algorithm allows a cave volume to evolve as a result of the in situ geomechanical conditions and the imposed production schedule. It has been validated at a number of different caving operations. The effect of the in situ geomechanical conditions and imposed production schedule on cave behaviour has been studied by conducting a series of numerical simulations of a conceptual block cave mine. The results are compared to traditional empirical methods for predicting caveability.

1 Introduction

It has long been recognised that the ability of an in situ rock mass to cave (or fragment) is a function of its strength in tension and shear and the value of the applied forces (after Brady and Brown, 2004). Cundall (2005) suggests that in order for a cave to propagate, the rock mass must be able to move downwards, which implies that the following events must occur; separation and or loosening in the crown, and; shearing distortion between the caved mass and the abutments. Both of these failure mechanisms require shear or tensile failure of the intact rock bridges as well as shearing and dislocation along pre-existing joints within a rock mass.

In recent years a numerical approach to the assessment of cave propagation has been developed in conjunction with the MMT project (Sainsbury et al., 2008a; Board and Pierce, 2009; Chitombo, 2010). The approach simulates cave propagation as a function of the specified draw strategy, evolving induced stress conditions and the simulated constitutive behaviour of the rock mass, without assumptions having to be made by the modeller regarding cave shape and the rock mass dilatation (bulking) response.

The numerical approach has been applied to a number of cave scenarios to provide an understanding of the sensitivities of a propagating cave to: a) rock mass strength; b) in situ stress; and c) simulated production draw. The results are presented in terms of propagation rate, bulking/dilation of the caved material, abutments stresses and predicted seismic potential.

2 Background

A conceptual model of caving has been developed by Duplancic and Brady (1999). The model includes four main behavioural regions that have also been defined within the numerical model of caving. A schematic diagram representing the relationship between the regions is presented in Figure 1. The characteristics of each region are:

- *Elastic Region* – The host rock mass around the caving region behaves mainly elastically. Rock mass behaviour and properties are those of an ‘undisturbed’ rock mass. Induced stresses in this region may be high enough to impact infrastructure.
- *Seismogenic Zone* – Microseismic (and sometimes seismic) activity will be concentrated in the region primarily due to discontinuity damage (discontinuities going from peak to residual strength) and the initiation of new fractures. Within the numerical model, the seismogenic zone is depicted by an empirically derived criterion developed by Diederichs (2000) and is described in detail in Reyes-Montes et al. (2010).

- *Yielded Zone* – The rock mass in this region is fractured and has lost some or all of its cohesive strength and provides minimal support to the overlying rock mass. Rock mass within the yielded zone will be subject to significant damage i.e. open holes will be cutoff, TDRs will break and cracking will be observable in infrastructure. Stress components within this region are typically low in magnitude.
- *Mobilised Zone* – This zone gives an estimate as to the portion of the orebody that has moved in response to the production draw and may be recoverable. Within the numerical model this has been defined as the 2 m displacement contour.
- *Air Gap* – The air gap shown in Figure 1A will exist only if the overlying yielded zone retains some level of cohesion. In caves under lower stress conditions, an air gap is interpreted to form within the numerical model when the yield zone becomes stationary and is coincident with the mobilised zone.

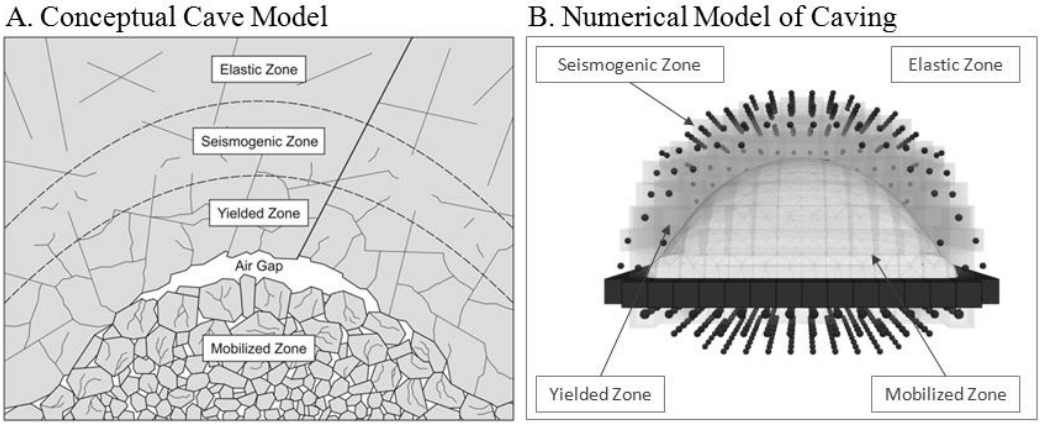

Figure 1 Main behavioural regions of a propagating cave

3 Rock mass constitutive behaviour

There is significant uncertainty regarding post-peak rock mass behaviour during the failure process and the manner in which the rock mass transitions from an intact to a caved material. In this complex process, creation of a propagating cave results in: a) deformation and stress redistribution of the rock mass above the undercut; b) failure of the rock mass in advance of the cave – with associated progressive reduction in strength from peak to residual levels; and c) dilation, bulking, fragmentation and mobilisation of the caved material. This overall response is often termed a 'strain-softening' process, and is the result of strain-dependent material properties.

In the caving model described herein, the strain-softening material is described by the Mohr–Coulomb failure criteria in which the post-peak strength behaviour is a function of plastic shear-strain-dependent rock mass cohesion and friction. The plastic shear strain required in going from peak strength to a fragmented rock mass (termed here the 'critical plastic strain') in the periphery of the cave defines the brittleness of the rock mass failure, and may be related to the Geological Strength Index (GSI) of the material and zone size within the model.

The bulking/dilation of rock mass that accompanies softening (resulting from the creation and opening of new fracture surfaces), as well as the corresponding decrease in density and modulus are accounted for within the model to ensure mass conservation (i.e. no mass is created or destroyed during the failure process). To achieve this balance, the density, modulus and dilatational response of the rock mass within the evolving cave volume are adjusted automatically to reflect the volumetric changes.

Large-scale numerical laboratory simulations with a strain softening model shows the progressive degradation of cohesion at various stages of unconfined compressive stress (UCS) sample loading, as illustrated in Figure 2(a). Previous simulations conducted by Sainsbury et al. (2008b) show how a numerical strain-softening response can be calibrated to observed failure modes and estimates of the complete rock mass stress–strain response derived from synthetic rock mass (SRM) testing. In lieu of SRM testing, peak

strength properties for the strain-softening material model can be estimated based on the measurable values of GSI, UCS, and m_i that may be used to develop a Hoek–Brown failure envelope and equivalent Mohr–Coulomb material properties. A bi-linear Mohr–Coulomb fit (presented in Figure 2(b)) to the Hoek–Brown curve can be used to more accurately represent the actual non-linearity of the failure envelope. In addition, the range of stress over which the Mohr–Coulomb properties are fit is limited to ensure a better match over the range of expected induced stresses during caving (as presented in Figure 2(c)).

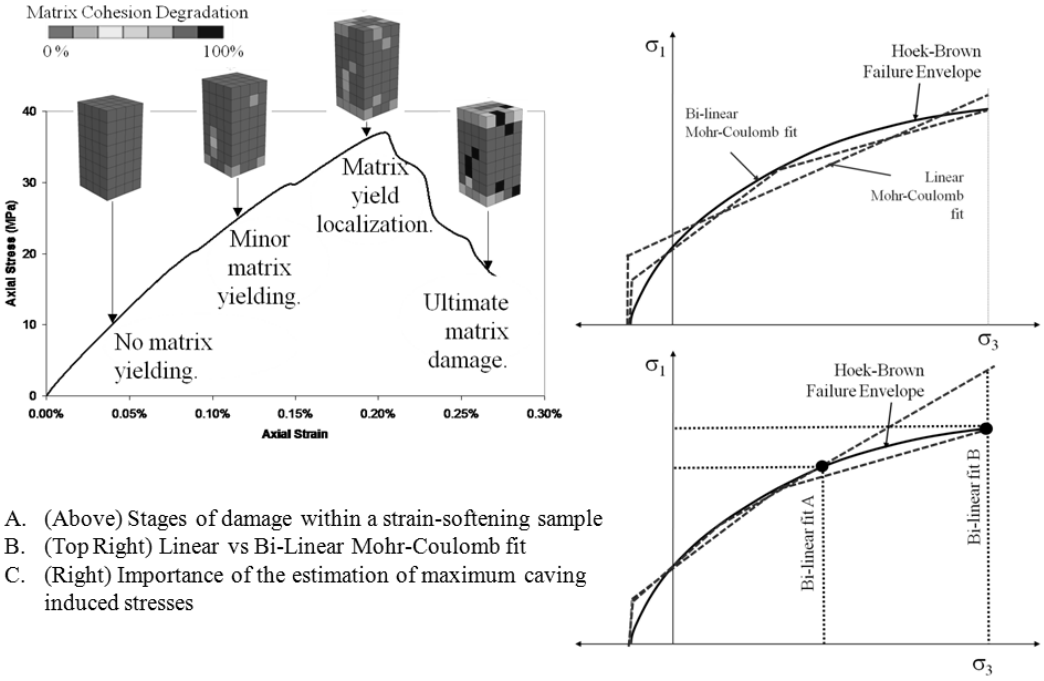

A. (Above) Stages of damage within a strain-softening sample
B. (Top Right) Linear vs Bi-Linear Mohr-Coulomb fit
C. (Right) Importance of the estimation of maximum caving induced stresses

Figure 2 a) Stages of damage within a strain-softening specimen; b) and c) development of Mohr–Coulomb strain-softening property estimates

4 Caveability sensitivity studies

Using the numerical model of caving, the sensitivity of cave behaviour in the early stages of production draw has been assessed based on variations in peak strength, post-peak response and production controls. The evolving cave behaviour has been analysed in terms of propagation rate, bulking/dilation of the caved rock mass, abutment stresses and seismic potential based on a criterion developed by Diederichs (2000) (discussed in Reyes-Montes et al. (2010)). It is important to note that a numerically derived seismogenic zone refers to the region in which intact rock failure may create acoustic output and does not necessarily represent the seismic response of known fault planes.

To investigate the effect of the in situ geomechanical conditions and imposed production schedule on cave behaviour, a simplified conceptual block cave mine has been simulated within the numerical modelling code FLAC3D (Itasca, 2009). The mining footprint has dimensions of 120 × 120 m (hydraulic radius (HR) of 30) and is located at a depth of 600 m below the ground surface. The maximum principal horizontal stress has been simulated at twice the vertical stress. Production has been simulated as a total height of draw (HOD) of 10 m.

To simulate the undercutting and production process within the numerical model, at the start of each advance increment, undercut zones are simulated with properties consistent with a fully fragmented and bulked caved material. Draw is simulated by applying a small downward oriented velocity to all grid points in the back of the undercut. This velocity is set low enough to ensure pseudo-static equilibrium throughout the model. By summing the masses drawn by all the grid points, the total production from the cave within the model can be calculated. Variability in the average draw velocity of 50% has been simulated over the entire mining footprint to simulate variations in drawbell production. A detailed description of the implementation of the

numerical caving algorithm is provided by Sainsbury et al. (2008b) and Board and Pierce (2009). A schematic representation of the conceptual numerical mine is provided in Figure 3(a).

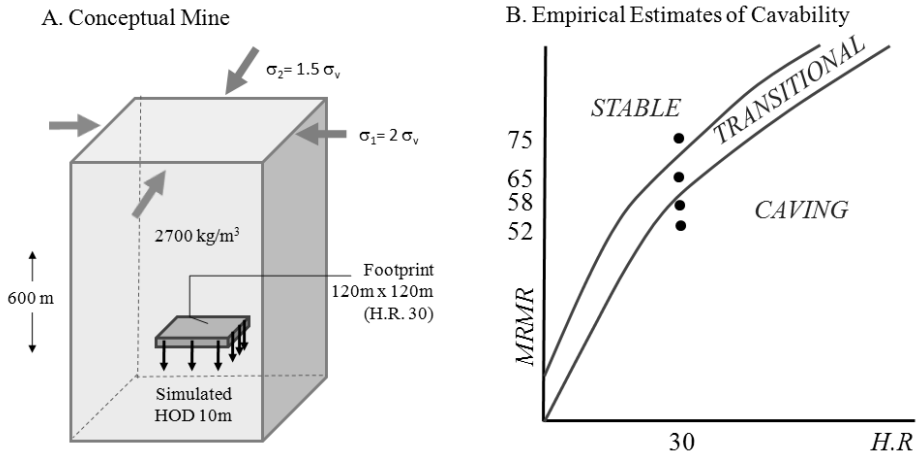

Figure 3 a) Conceptual block cave mine; b) empirical estimates of rock mass caveability

4.1 Rock mass peak strength

Four different strength rock masses have been defined (RM1, RM2, RM3 and RM4) and bi-linear, strain softening material responses have been developed for each based on the methodology described in Section 3. A summary of the measurable material properties and Mohr–Coulomb strength estimates for each of the rock masses are provided in Table 1 based on a maximum, minor principal stress fit of 15 MPa. The Hoek–Brown failure envelopes for each of the rock masses and stress–strain material responses at different confinement levels are provided in Figure 4.

Table 1 Estimate of Hoek–Brown and equivalent Mohr–Coulomb rock mass strength properties

							Seg. 1			Seg. 2	
	σ_{ci} (MPa)	GSI	MRMR	m_i	E_{rm} (GPa)	v	Tens. (MPa)	Coh. (MPa)	ϕ (Deg.)	Coh. (MPa)	ϕ (Deg.)
RM1	120	48	52	12	8.9	0.25	0.2	1.7	50	5.8	35
RM2	120	55	58	14	13.3	0.25	0.3	2.2	52	6.8	38
RM3	145	59	64	16	16.7	0.25	0.4	3.0	54	8.1	42
RM4	170	70	75	20	31.6	0.25	0.9	5.2	57	11.4	47

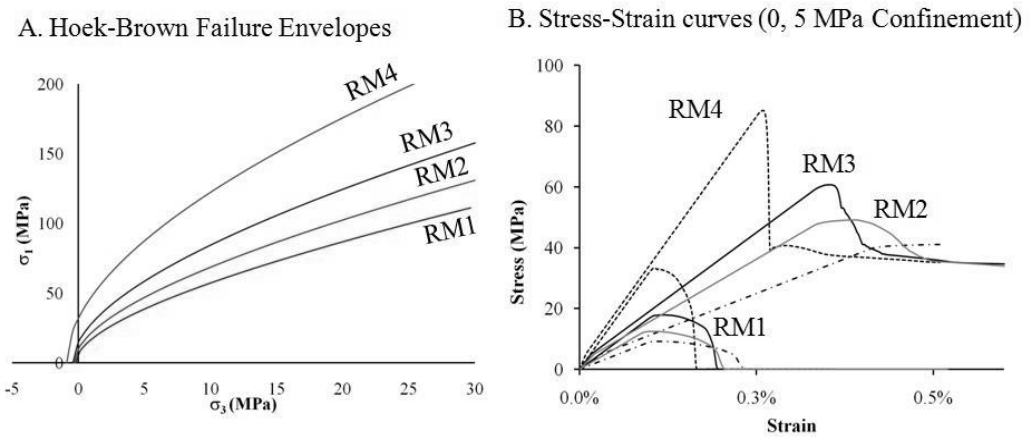

Figure 4 Hoek–Brown failure envelopes and simulated rock mass stress–strain curves

The empirical estimates of caveability (after Laubscher, 2000) for each of the rock masses are provided in Figure 3(b). Each of the rock masses are classified as having a different caveability potential based on their mining rock mass ration (MRMR) values — assuming the simulated conceptual mine HR of 30. The RM4 rock mass falls within the stable region which suggests that cave initiation and propagation may be problematic (based on operational experience with similar rock mass types at other mines). Caving in the RM1 and RM2 rock masses is not expected to be problematic. Based on previous experience with similar type rock masses to RM3, the caveability is unable to be determined since it falls within the Transitional Zone. The numerical simulations results for a block cave developed within each of the rock masses are provided in Figure 5.

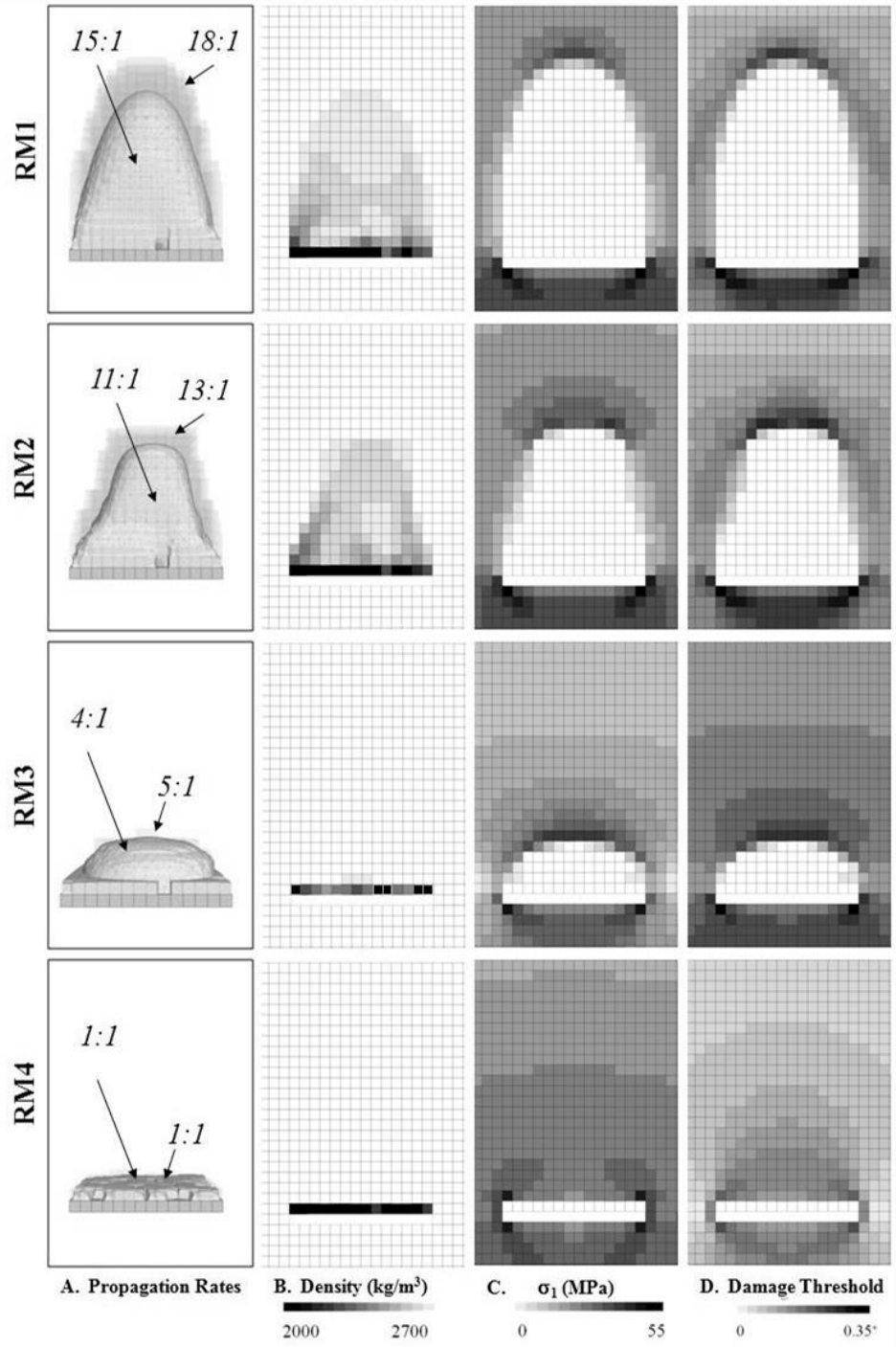

Figure 5 Cave simulation results for variable peak strength rock masses

It can be seen that as the rock mass strength increases, the propagation rate decreases. Continuous cave propagation in the lower strength RM1 and RM2 rock masses is predicted. Stalling is seen in the simulation of caving in RM3 (depicted by the coincident cave and yield zones in Figure 5A). The cave fails to initiate in RM4. The propagation rates simulated in the numerical model are consistent with those that have been reported at operating mines around the world (presented in Table 2).

Table 2 Summary of published propagation rates from operating mines

Operation	Cave Method	Yield Propagation Rate	Reference
El Teniente, Chile	Panel	5:1	Villegas (2009, written comm.)
Henderson Mine, Colorado, USA	Panel	7:1	Board and Pierce (2009)
Grace Mine, Pennsylvania, USA	Panel	8.2:1	Sainsbury (2005)
Australian Coal Mines	Longwall	8.9:1	UNSW (1995)
Deep Ore Zone Mine, Indonesia	Block	6–10:1	Szwedzicki et al. (2005)
Kimberley Mines, South Africa	Block	6–12:1	Guest (2009, written comm.)
Lakeshore Mine, Arizona USA	Block	10:1	Panek (1984)
Questa Mine, New Mexico, USA	Block	10:1	Gilbride et al. (2005)
San Manuel Mine, Arizona, USA	Panel	10:1	Gilbride et al. (2005)
Athens Mine, Michigan, USA	Block	14:1	Boyum (1961)
Palabora Mine, South Africa	Block	15:1	Sainsbury et al. (2008b)
Northparkes Lift 2 Mine, Australia	Block	20:1	Pierce et al. (2006)
Chinese Coal Mine	Longwall	31.3:1	Liu (1981)

The evolution of the bulked caved mass for each rock mass is presented in Figure 5B. It can be seen that bulking is not uniform within the caved mass. Higher bulking (lower densities) can be seen at the edges of the cave. Results of the RM4 model provide a full-bulked caved rock across the entire mining footprint, while the RM1 and RM2 rock masses only reach a maximum bulked rock mass density around the cave periphery – where the shearing stress is at a maximum. These results are considered to represent more closely the actual dilatational response of a rock mass during caving than assuming a constant reduced density for production calculations.

Maximum principal stress magnitudes (shown in Figure 5C) in the mining abutments of the lower strength RM1 and RM2 rock masses reach larger values than the higher strength RM3 and RM4, minimal stress redistribution has occurred in the high strength cases. It is expected with the additional simulation of production draw, abutments stresses will continue to increase in the RM1 and RM2 models until the cave intersects the ground surface.

The Damage Threshold values plotted for each of the rock masses provide two important pieces of information that include a) if damage is occurring in the rock mass and b) where this damage is occurring. This is important in understanding the ongoing caveability of the rock mass and where the cave shape is likely to evolve. The results provided in Figure 5D shows that seismicity within the lower strength rock mass is higher (since the damage threshold will be reached at lower induced stresses) both in the cave back (suggesting continued propagation of the cave), and at the extraction level.

The simulation of caving in each of the rock mass types agree with the initial estimates of caveability based on Laubscher's (2000) caveability chart for a simplified conceptual cave. However, as shown through the

subsequent sensitivity analyses, simulated cave behaviour can vary significantly based on the variation of the in situ geomechanical conditions and imposed mining strategy.

4.2 Post-peak softening rate

The rate at which the degradation from the in situ to caved state occurs within a rock mass is referred to as the post-peak brittleness. Lorig (2004) has shown, through numerical simulations of caving in 2D, that cave height is strongly dependant on the brittleness of the rock mass. In lieu of SRM testing (Pierce et al., 2006) results to provide an estimate of post-peak brittleness, the response can be estimated based on a relationship with GSI and zone size within the numerical model. In general it is assumed that high GSI values will correlate to a more brittle post-peak response since more intact failure will be involved in the failure process. The effect of variable post-peak brittleness on cave performance has been studied by modifying the post-peak response of the RM1 rock mass. The stress–strain results of large-scale laboratory simulations that represent a ductile, average, and brittle post-peak response for RM1 are provided in Figure 8. Each of the rock mass responses have been developed based on the same peak strength properties (i.e. same Hoek–Brown failure envelope and Mohr–Coulomb properties). The only difference is the plastic shear strain required to reduce the strength of the rock mass from a peak to residual value.

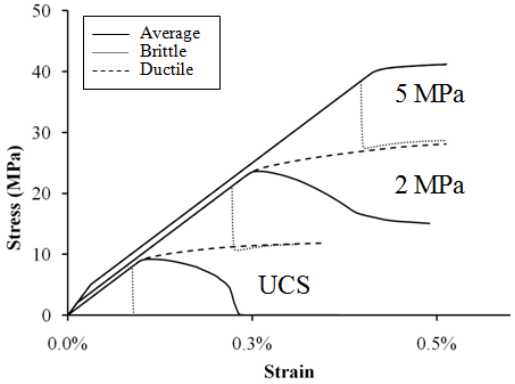

A. (Left) Simulated stress-strain responses
B. (Below) Critical plastic strain variance

Post-Peak Response	Critical Plastic Strain
Brittle	6.3e-5
Average	6.3e-3
Ductile	6.3e-1

Figure 6 a) Simulated variable post-peak softening responses; b) critical plastic strain variance

It can be seen in Figure 7A that the cave propagation rate is strongly influenced by the post-peak response of the rock mass. The propagation rate within the numerical model is calculated based on the ratio of cave back height to simulated production HOD. Problematic cave initiation and propagation is simulated with a ductile post-peak response for RM1. Similar propagation rates are simulated for the average and brittle post-peak responses, however, it can been seen that, as the brittleness increases, the advance of the yield zone in front of the mobilised zone also increases from 10–30 m up to 40–50 m. The lateral extents of the yield zone (beyond the mining footprint) are also increased in the case of the brittle response.

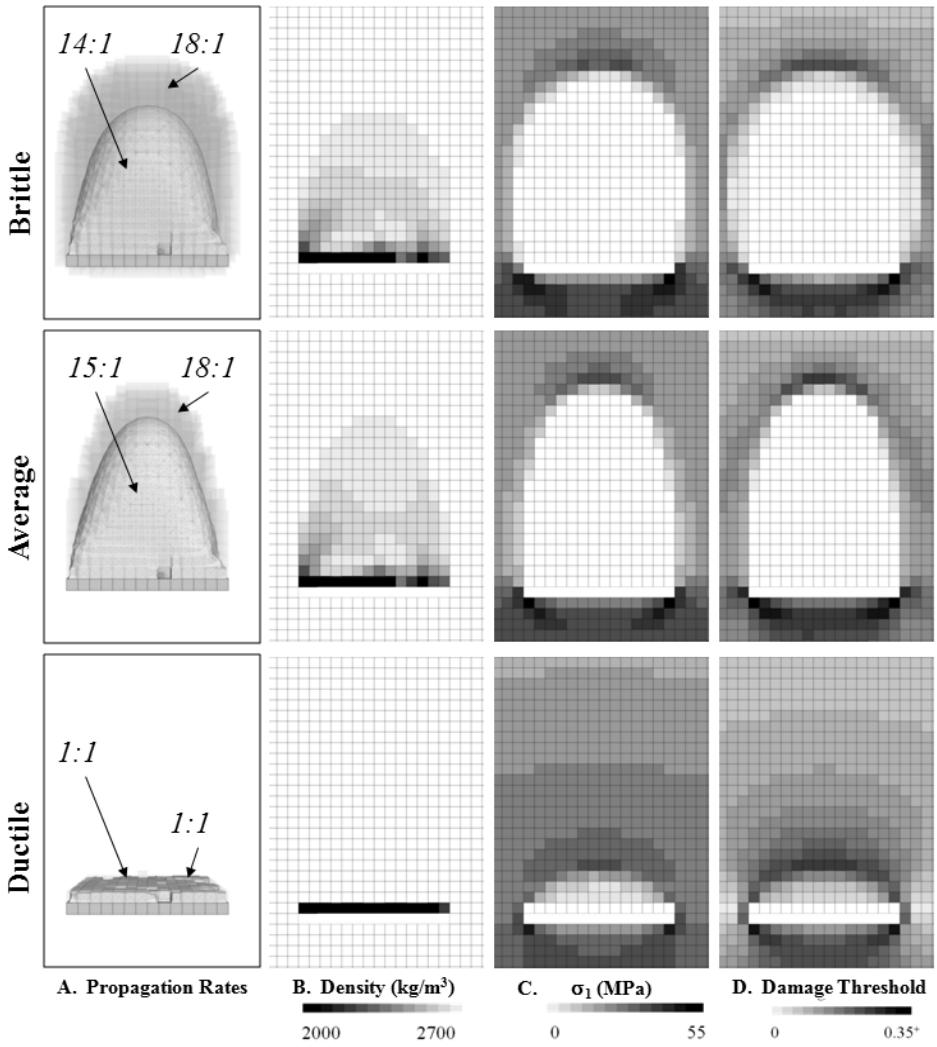

Figure 7 Cave simulation results for variable post-peak softening rates

4.3 Estimate of m_i value

The Hoek–Brown m_i constant is an intact property that varies with rock type and is used to estimate rock mass strength. It is a measure of strength gain with confinement and can be determined from laboratory triaxial testing. This parameter can be difficult to define, and is often estimated based upon empirical values which have significant variance. The effect of the assumed m_i value on the simulated caving response has been studied by modifying the failure envelope for the RM1 rock mass to reflect m_i material constant values of 5, 12 and 25. The resultant Hoek–Brown failure envelopes and equivalent bi-linear Mohr–Coulomb strength properties are presented in Figure 8.

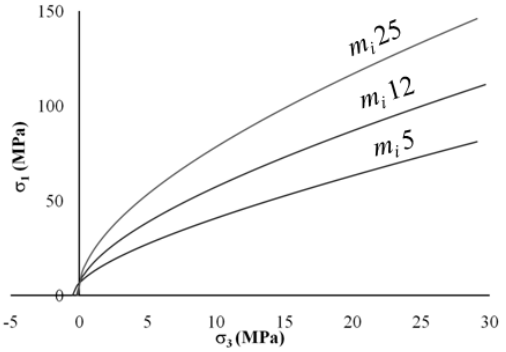

A. (Left) Hoek-Brown Failure Envelopes
B. (Below) Equivalent Mohr-Coulomb properties

	Seg. 1			Seg. 2	
	Tens.	Coh.	ϕ	Coh.	ϕ
m_i	(MPa)	(MPa)	(Deg.)	(MPa)	(Deg.)
5	0.5	1.9	40	4.7	27
12	0.2	1.4	53	4.0	40
25	0.1	1.7	57	7.0	42

Figure 8 a) Hoek–Brown curves; b) equivalent bi-linear Mohr–Coulomb property estimates

Figure 9A illustrates that an increase in the estimated m_i reduces (marginally) the propagation rate of a cave. This decrease can be attributed to the increased stress at which failure must occur (based on Figure 8) with increasing m_i values. In each case, the bulked cave mass profiles (Figure 9B) are similar. Increased seismic potential — based on the empirically derived equation developed by Diederichs (2000) — within the cave back is predicted with an increased m_i (Figure 9D). This reflects the stress caving mechanism associated with the propagation of strong rock masses.

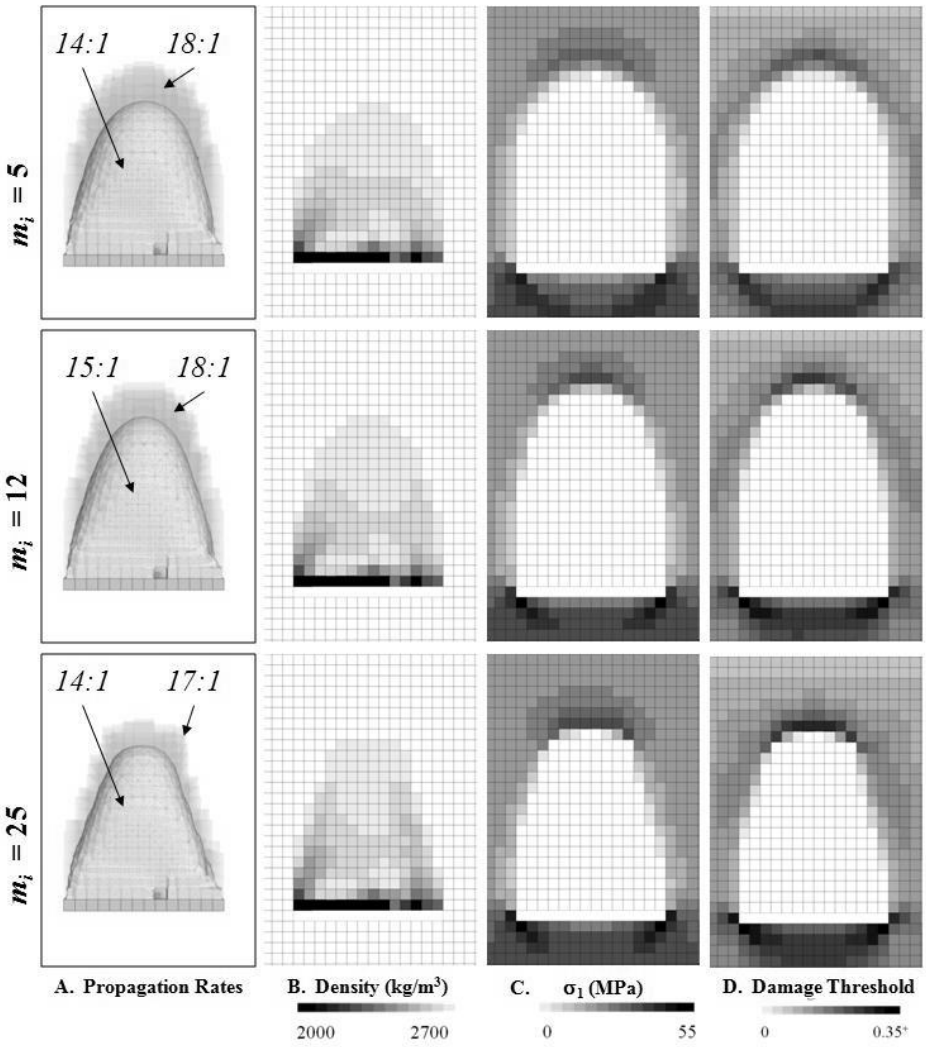

Figure 9 Effect of m_i on the caveability of a rock mass

4.4 Effect of stress/depth

During cave propagation, in situ stresses are redistributed around the evolving caved mass. The effect that the in situ stress magnitude has on the evolving cave has been investigated by simulating the base case mining scenario (where the in situ horizontal stresses were 1.5 and two times the vertical stress) at different depths. The RM1 rock mass properties have been simulated. It can be seen from Figure 10A and Figure 10D that, the cave propagation rate, and seismic potential increases with increased stress/depth. In addition, as the stress magnitude increases, the rate of the advance of the yield zone in front of the mobilised zone also increases (Figure 10A).

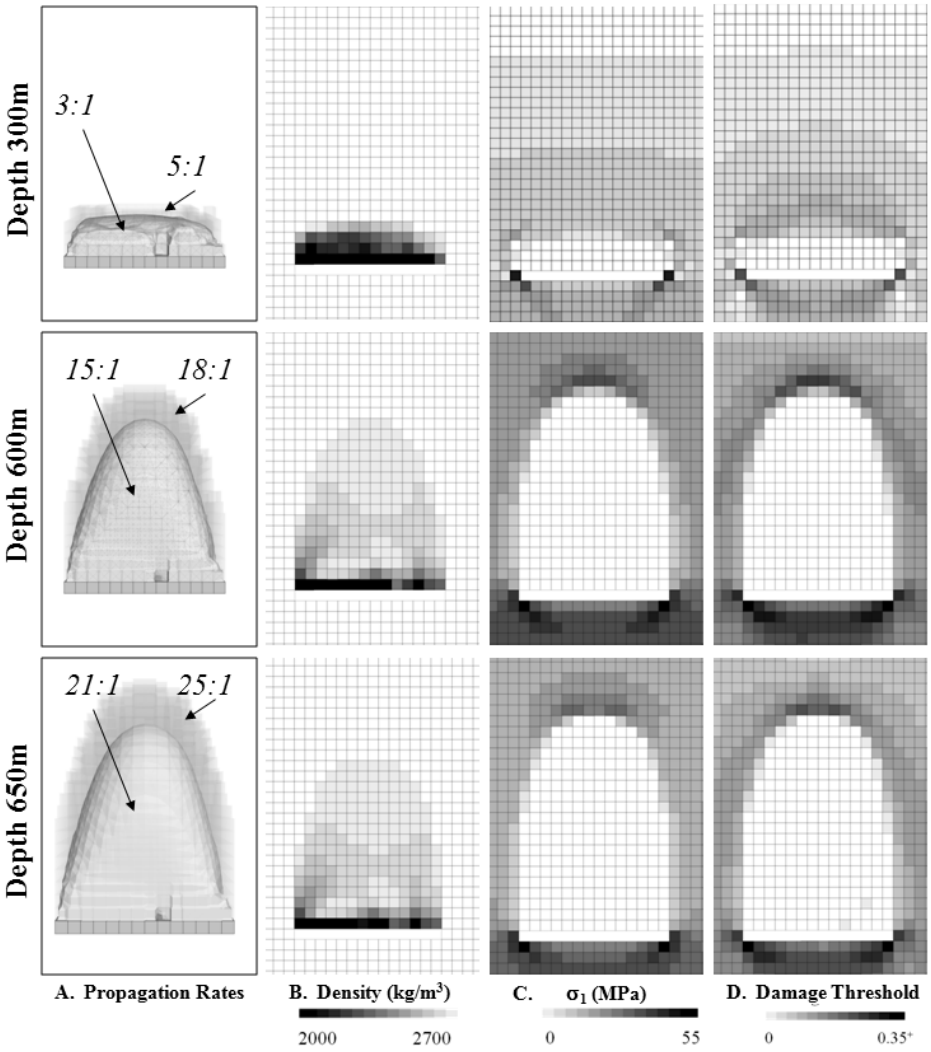

Figure 10 Cave simulation results for increasing stress/depth

4.5 Maximum bulking potential

When caving occurs, due to the translation and rotation of rock blocks, the rock mass bulks/dilates and occupies a greater volume than its in situ state. The term bulking factor (B) defines the volumetric ratio of the bulked (or broken) rock to solid in situ rock and is known to vary with rock mass type. Highly laminated rocks like mudstone or shale typically have a low B value whereas; stronger more massive rock mass types like sandstone generally have a higher B value. When rock is drawn from a propagating cave, confinement is progressively removed from the rock mass and it displaces into the excavation (becomes part of the mobilised zone). The effect that the maximum bulking factor has on the cave shape has been investigated by reducing the maximum allowable bulking factor of RM1. The results of the simulations are provided in Figure 11.

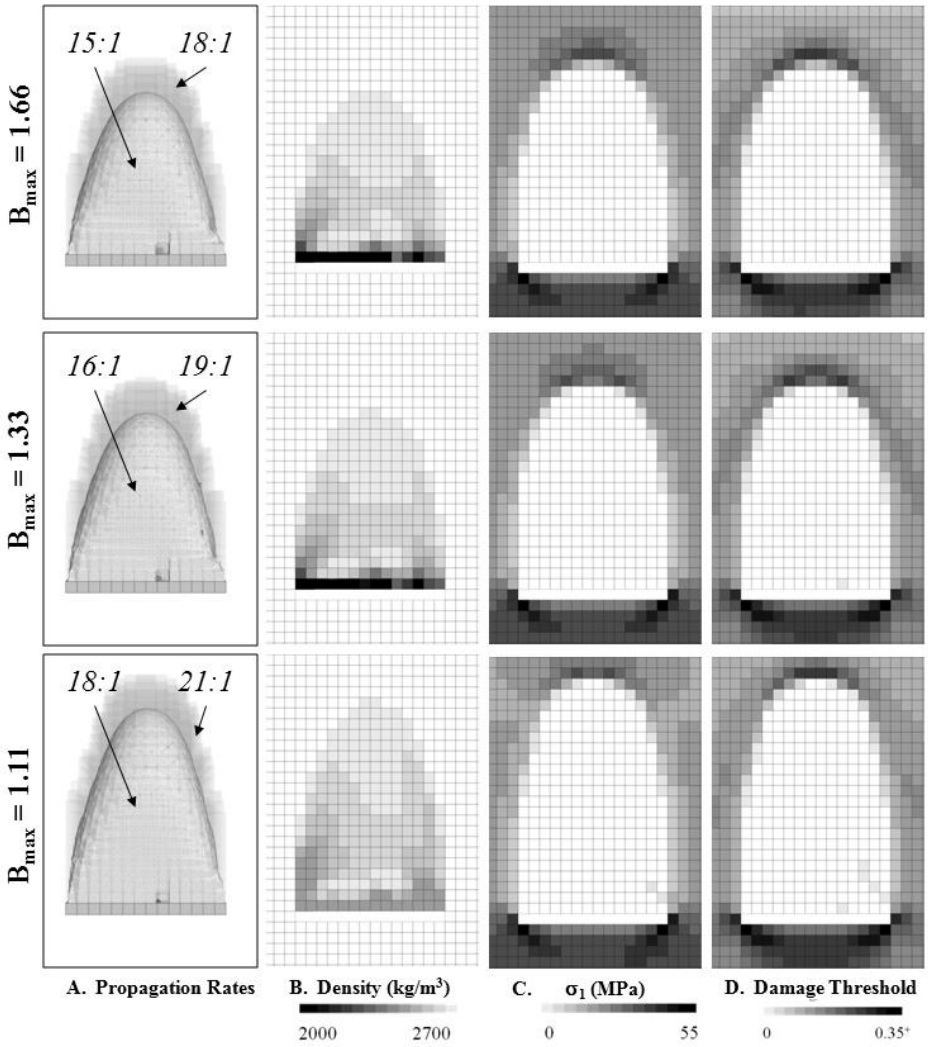

Figure 11 Cave simulation results for variable maximum bulking rates

It can be seen from Figure 11A, that as the maximum bulking factor of a rock mass decreases, the cave propagation rate increases.

4.6 Effect of draw strategy

When planning a cave mine, there are a number of production controls that can be implemented to ensure optimum cave performance. The effect that the implemented production schedule has on cave performance has been considered by simulating a) uniform draw and b) incremental draw. For each of these scenarios an average height of draw of 10 m has been achieved across the entire mining footprint. The simulation results are provided in Figure 12.

By simulating perfectly uniform draw (zero variability in drawbell production), an increase in the propagation rate is seen in Figure 12A since; shear stresses within the caved mass will be decreased, resulting in a reduction of the bulking of the rock mass. The effect that a uniform draw strategy has on a cave propagation rate has been documented by Pierce et al. (2006) during a numerical back analysis of the Northparkes Lift 2 cave behaviour. In addition, by staggering production and simulating an incremental draw strategy (where mining areas are progressively brought online) the resulting propagating cave rate is decreased as this induces greater shear stresses within the caved mass, resulting in increased rock mass bulking.

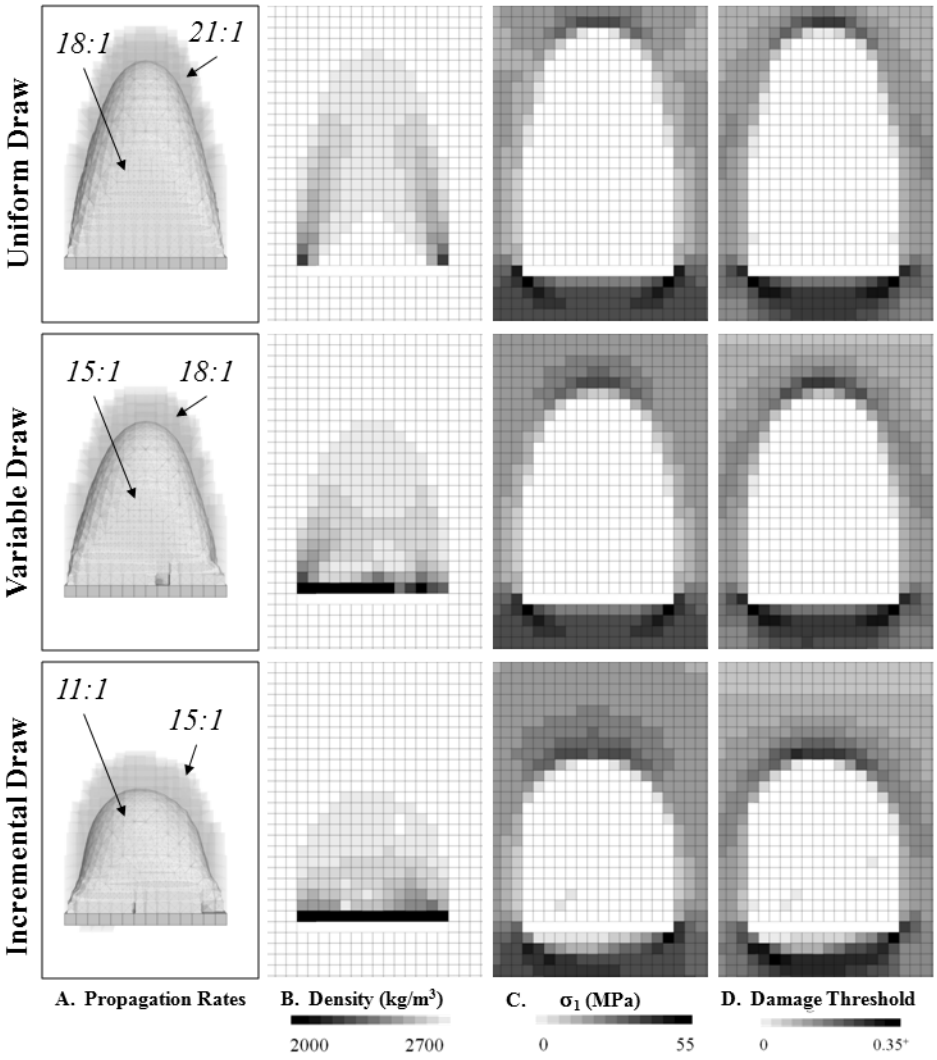

Figure 12 Effect of draw strategy on the caveability of a rock mass

5 Conclusions

A numerical approach to modelling of caving has been developed within the industry funded MMT project. The caving algorithm, allows cave propagate to evolve as a function of the constitutive behaviour of the rock mass, induced stress conditions and the specified draw strategy.

The cave behaviour of a conceptual block cave mine has been simulated with different rock masses with increasing strength. The numerical simulations provide a good correlation with empirical estimates of caveability. However, the numerical assessment of caving provides a much greater understanding of cave propagation and the effect of various geomechanical parameters not considered in empirical caveability techniques.

It has been demonstrated that variations in the in situ stress, post-peak brittleness, m_i values, maximum bulking factors and simulated draw strategy can have a significant effect on the cave behaviour of a particular rock mass.

Acknowledgements

The author would like to thank the sponsors of the MMT project for their continued support of fundamental caving mechanics research. Thanks also go to Itasca, and in particular, the author's co-collaborators in most cave simulations (Mr Matt Pierce and Dr David Sainsbury).

References

Brady, B. and Brown, B. (2004) Rock mechanics for underground mining, Third Edition, Dordrecht, London, Kluwer Academic Publishers 2004, xviii, 626 p.

Board, M. and Pierce, M. (2009) A review of recent experience in modelling of caving, International Workshop on Numerical Modeling for Underground Mine Excavation Design June 28, 2009 Asheville, North Carolina in conjunction with the 43rd U.S. Rock Mechanics Symposium.

Boyum, B.H. (1961) Subsidence Case Histories in Michigan Mines, Fourth Rock Mechanics Symposium, Pennsylvania State University.

Chitombo, G. (2010) Cave mining — 16 years after Laubscher's 1994 paper 'Cave mining – state of the art', in Proceedings 2nd International Symposium on Block and Sublevel Caving (Caving 2010), Y. Potvin (ed), 20–22 April 2010, Perth, Australia, Australian Centre for Geomechanics, Perth, pp. 45–62.

Cundall, P.A. (2005) Caving Mechanics Task 1-Scoping Study, Report to MMT Technical Director, Julius Kruttschnitt Mineral Resource Centre.

Duplancic, P. and Brady, B.H. (1999) Characterization of caving mechanisms by analysis of seismicity and rock stress, in Proceedings 9th International Congress on Rock Mechanics, Paris, Balkema, Rotterdam, Vol. 2, pp. 1049–1053.

Diederichs, M.S. (2000) Instability of Hard Rockmasses: The Role of Tensile Damage and Relaxation, PhD Thesis, University of Waterloo, 617 p.

Gilbride, L., Free, K. and Kehrman, R. (2005) Modeling Block Cave Subsidence at the Molycorp Inc., Questa Mine – A Case Study, Alaska Rocks 2005, in Proceedings 40th U.S. Symposium on Rock Mechanics (USRMS), June 25–29, Anchorage, 14 p.

Itasca Consulting Group, Inc. (Itasca) (2009) FLAC3D – Fast Lagrangian Analysis of Continua in 3 Dimensions, User's Manual, Minneapolis, Itasca, Ver. 4.

Laubscher, D.H. (2000) Block Caving Manual, Prepared for the International Caving Study, Julius Kruttschnitt Mineral Resource Centre and Itasca Consulting Group, Brisbane.

Lorig, L. (2004) The role of numerical modelling in assessing caveability, International Caving Study, 2004.

Lui, T.Q. (1981) Surface Movements, Overburden Failure and its Applications, Coal Industry Publishing, China.

Panek, L.A. (1984) Subsidence in undercut-cave operations, subsidence resulting from limited extraction of two neighboring cave operations, in Geomechanical applications in hard rock mining, W.G. Pariseau (ed), pp. 225–240.

Pierce, M., Young, P., Reyes-Montes, J. and Pettitt, W. (2006) MMT Project Caving Mechanics Report, ICG06-2292-1-T3-40.

Sainsbury, B., Pierce, M. and Mas Ivars, D. (2008a) Analysis of Caving Behaviour Using a Synthetic Rock Mass — Ubiquitous Joint Rock Mass Modelling Technique, in Proceedings 1st Southern Hemisphere International Rock Mechanics Symposium (SHIRMS), Y. Potvin, J. Carter, A. Dyskin and R. Jeffrey (eds), Australian Centre for Geomechanics, Perth, Australia, Vol. 1 – Mining and Civil, pp. 243–254.

Sainsbury, B., Pierce, M. and Mas Ivars, D. (2008b) Simulation of rock mass strength anisotropy and scale effects using a Ubiquitous Joint Rock Mass (UJRM) model, in Proceedings First International FLAC/DEM Symposium on Numerical Modelling, Minneapolis, USA, Minneapolis: Itasca.

Sainsbury, D.P. (2005) Investigation of Mining-Induced Subsidence at the Abandoned Grace Mine, Confidential Itasca report to New Morgan Properties, L.P. ICG04-2262-29.

Szwedzicki, T., Widijanto, E. and Sinaga, F. (2006) Propagation of a Caving Zone, A Case Study from PT Freeport, Indonesia, in Proud to Be Miners (MassMin 2004, Santiago, August 2004), Santiago: Mineria Chilena.

Reyes-Montes, J., Sainsbury, B., Pettitt, W. and Young, P. (2010) Microseismic tools for the analysis of the interaction between open pit and underground developments, in Proceedings 2nd International Symposium on Block and Sublevel Caving (Caving 2010), Y. Potvin (ed), 20–22 April 2010, Perth, Australia, Australian Centre for Geomechanics, Perth, pp. 119–132.

UNSW (1995) UNSW Pillar Design Outcomes, Issue No. 7, The University of New South Wales.